Volume 1 | Number 1 | Jan 2013 | Pages 1–100

Journal of
Materials Chemistry A

Materials for energy and sustainability
www.rsc.org/materialsA

ROYAL SOCIETY
OF CHEMISTRY

ROYAL SOCIETY
OF CHEMISTRY

www.rsc.org/materialsA

The Role of Conjugated Side Chains in High Performance Photovoltaic Polymers

Meng Wang[1,2], Di Ma[1], Keli Shi[1,3], Shaowei Shi[1], Song Chen[4], Changjiang Huang[1], Zi Qiao[1], Zhi-Guo Zhang[3], Yongfang Li[3]*, Xiaoyu Li[1]*, and Haiqiao Wang[1.2]*

1.   State Key Laboratory of Organic-Inorganic Composite, Beijing University of Chemical Technology, Beijing 100029, China

2.   Key Laboratory of Carbon Fiber and Functional Polymers, Ministry of Education, Beijing University of Chemical Technology, Beijing 100029, China

3.   Beijing National Laboratory for Molecular Sciences, Institute of Chemistry, Chinese Academy of Sciences, Beijing 100190, China

4.   China Textile Academy, Beijing, 100025, China

Corresponding author: e-mail: wanghaiqiao@mail.buct.edu.cn (H. Wang); liyf@iccas.ac.cn (Y. Li); lixy@mail.buct.edu.cn (X. Li)

ABSTRACT: Four new D-A type copolymers, namely PBDT-DFQX-PP, PBDT-DFQX-TP, PBDT-DFQX-PT and PBDT-DFQX-TT, were designed and synthesized to investigate the influence of conjugated side chain pattern on photovoltaic properties of conjugated polymers. All the four copolymers have an identical conjugated backbone comprising benzo[1,2-b:4,5-b']dithiophene (BDT) donor unit and quinoxaline (Qx) acceptor unit, but with varying conjugated side chains, *p*-alkoxyphenyl or 2-alkylthienyl, attached to the donor and acceptor

units, respectively. As evidenced by UV/Vis absorption spectra, electrochemical cyclic voltammetry, density functional theory (DFT), grazing incidence X-ray scattering (GIXS), transmission electron microscope (TEM) and photovoltaic measurements, the difference in conjugated side chain modulation led to totally different physicochemical properties. Among the four copolymers, PBDT-DFQX-TT exhibits the broadest absorption spectrum, most closed packed structure as well as a finest fibril structure when blended with $PC_{71}BM$. After systematic device optimization, the power conversion efficiencies (PCEs) of the bulk heterojunction (BHJ) photovoltaic devices based on the blends of PBDT-DFQX-PP, PBDT-DFQX-TP, PBDT-DFQX-PT and PBDT-DFQX-TT with $PC_{71}BM$ achieved 3.96%, 6.08%, 6.54% and 7.68%, respectively. By systematic varying the side chains of the copolymers from all phenyl groups to all thienyl ones, PCEs was increased by 250% from 3.96% to 7.68%. To date 7.68% is one of a few Qx-based PSCs which exhibited PCE exceeding 7.5%, and the results suggest that modulating the conjugated side chains on donor and acceptor units of copolymers simultaneously would be an effective strategy for constructing high performance photovoltaic copolymers.

INTRODUCTION

Bulk-heterojunction (BHJ) polymer solar cells (PSCs) based on conjugated polymer donor and fullerene derivative acceptor are promising devices for alternative energy sources because of their potential applications in flexible, light-weight, and low-cost large-area solar cells through roll-to-roll printing.[1] Stimulatingly, recent advances in the power conversion efficiencies (PCEs) of solution-processed PSCs have exceed 9% for single-junction devices,[2] owing to the development of new donor materials, engineered interfaces and enhanced control of polymeric film microstructure. Nowadays, the majority of synthetic efforts and structure-property studies in the field have been devoted to the new low band-gap donor-acceptor (D-A) copolymers, which

could be easily tuned to feature broad absorption spectra, high charge carrier mobilities and suitable energy levels by selecting different donor or acceptor units. Low band-gap D-A copolymers have been successfully used in achieving both a high short-circuit current (J_{sc}) and a high open-circuit voltage (V_{oc}) simultaneously, leading to enhanced PCEs.[3]

Generally a conjugated polymer can be arbitrarily divided into two constituting components: the π-conjugated backbones and the side chains, where π-conjugated backbones mainly determine the optoelectronic properties of the resulting polymers. Consequently hundreds of different backbones have been reported so far.[4] On the other hand, selecting the side chains is as important as selecting the conjugated backbones when designing conjugated polymers. The side chain engineering is indeed an essential and widely spread technique used to tune the physical properties of a conjugated polymer, including absorption, emission, energy level, molecular packing, and charge transport. Currently, the majority of reports on the side chain engineering focused either on the donor units or on the acceptor units individually. For instance, Hou and co-workers[2a] recently reported the syntheses and study of 2D-conjugated polymers base on BDT and thienothiophene (TT) units, in which only the donor units have varying furan, thiophene or selenophene side groups, while the acceptor units kept no change, and the resultant copolymers exhibited totally different photovoltaic properties due to change of the conjugated side chains on the donor units. In addition, some similar works were reported by Cao[5a] and K-H Wei[5b] (see Scheme 1). However, upon further inspection of the follow-up works, we found that very limited study concentrated on those copolymers, in which the donor and acceptor units have conjugated side chains simultaneously, and synergistic effect of the conjugated side chains is scarcely taken into account to date.[6] Whereas, it seems that adjusting the conjugated side chains on donor and on acceptor units synchronously could be more effective method for tuning the film forming

properties, steric hindrance, π-π stacking and microstructure of the active layer in BHJ. Therefore, it is of interest to investigate the synergistic effect of conjugated side chains on both donor and acceptor units on polymer photovoltaic properties in an effort to further understand the structure-property relationships.

As well-known, amongst the various acceptor monomers utilized, quinoxaline (Qx) is a strong electron acceptor unit widely used as building block for optoelectronic applications, since it can be easily modified and side substituted to finely tune the optoelectronic properties of the resulting polymer.[7] On the other hand, benzodithiophene (BDT) is one of the most promising electron donor units for photovoltaic applications thanks to its desirable peculiarities such as structural rigidity and planarity and favorable inter-chain π-π stacking, other than the presence of additional substitution sites for the incorporation of side chains.[8] The feature of easy modification of BDT and Qx provides a selectivity to construct polymers through dual side chain modulation. It has been recently demonstrated that use of a vertical π-conjugation extension on the Qx-based polymers can dramatically increase the PCE.[9] Thus, how to select conjugated side chain combination to achieve high efficiency of BDT-DFQX-based PSCs is an important and challenging issue.

Prompted by the above considerations, herein, we designed and synthesized four new *p*-type conjugated D-A copolymers, PBDT-DFQX-PP, PBDT-DFQX-TP, PBDT-DFQX-PT and PBDT-DFQX-TT (whose molecular structures are shown in Scheme 2) based on benzodithiophene (BDT) donor unit and fluorinated quinoxaline (DFQX) acceptor unit. The conjugated side chains both on donor and on acceptor units of these copolymers were varied from *p*-alkoxyphenyl to 2-alkylthienyl in turn, in order to investigate the effect of location and kind of the conjugated side chains on morphology, charge transport and photovoltaic performance of the

copolymers. Owing to the difference in electron-donating ability, aromaticity, delocalization and planarity, *p*-alkoxyphenyl (P) or 2-alkylthienyl (T) side group was chosen to tune the solubility, energy level and the chain packing of the polymers. In addition, electron-withdrawing fluorine substitutions were employed to further decrease HOMO energy levels and enhance the interchain interaction of the BDT-DFQX copolymers. As evidenced by UV/Vis absorption spectra, X-ray diffraction (XRD), grazing incidence X-ray scattering (GIXS) and transmission electron microscope (TEM), PBDT-DFQX-TT with all thienyl side chains possesses the highest ordered structure with the best planarity and tightest molecular packing, therefore, the PSC based on its blend with PC$_{71}$BM achieved the promising PCE of 7.68% with an exceptional fill factor of about 70%. Whereas the device based on PBDT-DFQX-PP with all phenyl side chains just exhibited a moderate PCE of 3.96%. These results demonstrate that modulating the conjugated side chains both on donor and on acceptor units of copolymers simultaneously is an effective way for constructing high performance photovoltaic copolymers.
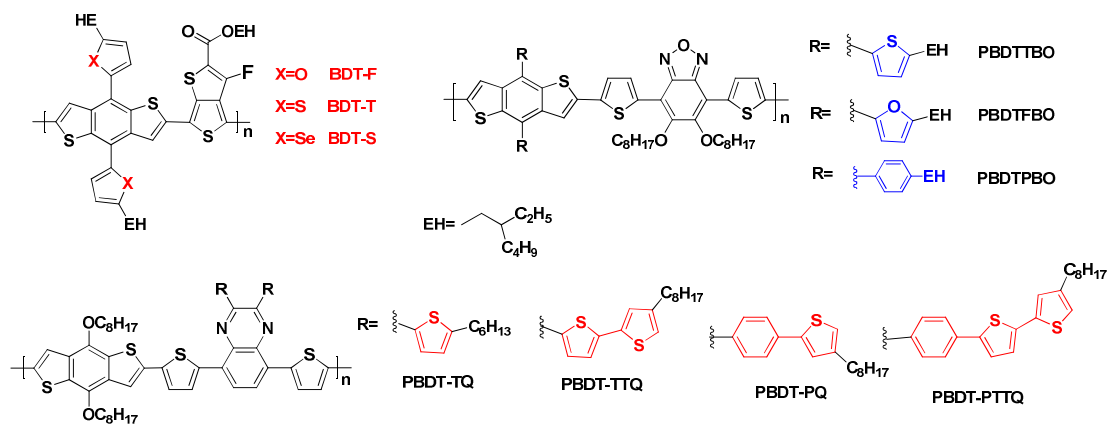
Scheme 1. Chemical structures of copolymers with varied side groups reported in literature.

Scheme 2. Molecular structures of designed BDT-DFQX-based copolymers with different conjugated side chains.

6
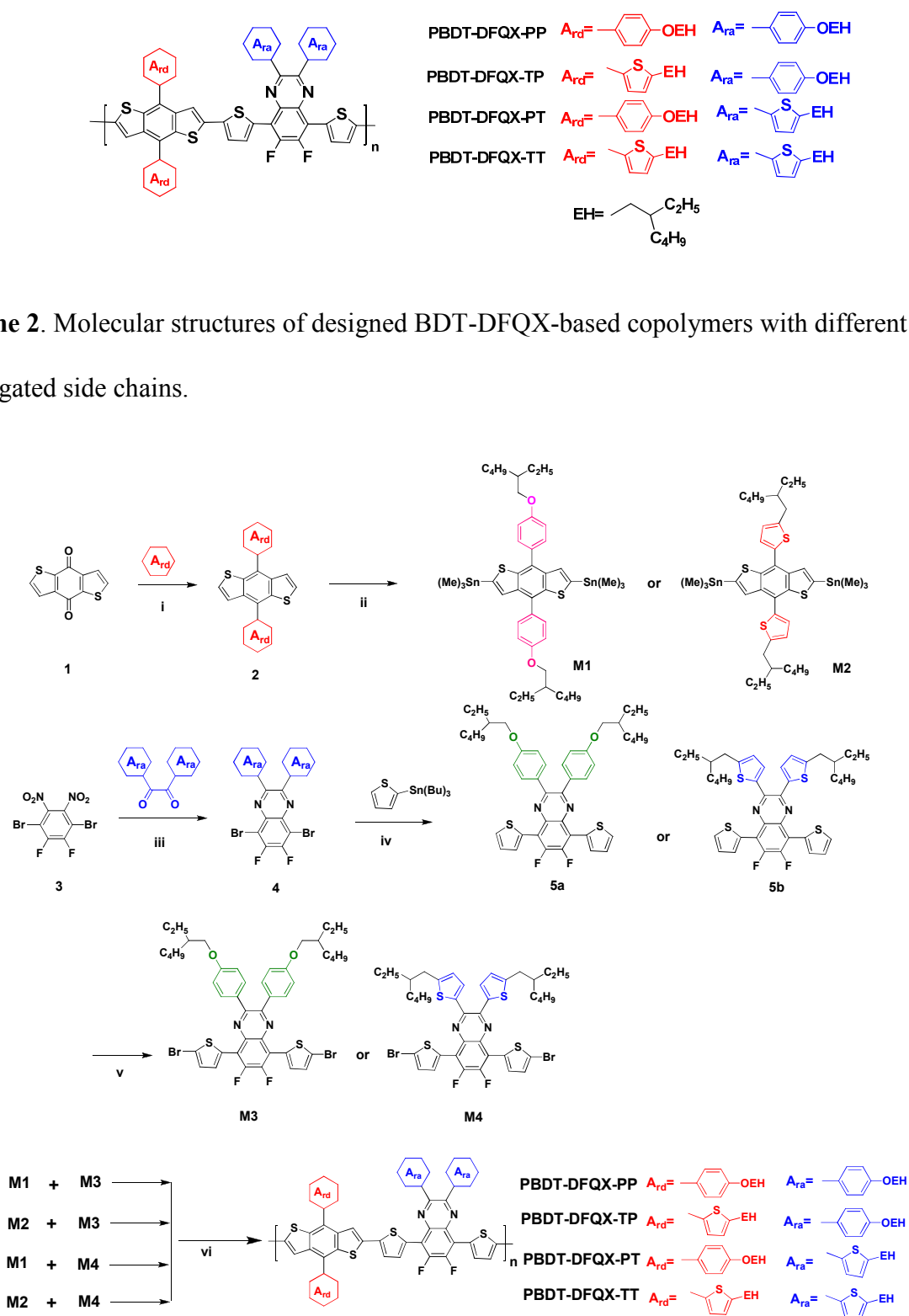
Scheme 3. Synthetic routes of the monomers and the corresponding copolymers. (i) 0°C, 15

min and then 50°C, 30 min; SnCl$_2$/HCl/H$_2$O, 50°C, 1 h. (ii) n-Butyllithium, -78°C, 30 min;

trimethyltin chloride, ambient temperature, 30 min. (iii) Fe, CH$_3$COOH, reflux, 12 h. (iv)

PdCl$_2$(PPh$_3$)$_2$, 120°C, 24 h. (v) NBS, THF, ambient temperature,12h. (vi) Pd$_2$(dba)$_3$/P(*o*-tol)$_3$,

130°C, 48h.

RESULTS AND DISCUSSION

Synthesis and Characterization.

The synthesis routes for copolymers are depicted in Scheme 3. For donor moiety, starting from

benzo[1,2-b:4,5-b']dithiophene-4,8-dione **1**, a Grignard reagent synthesis afforded compound **2a**

or **2b**. Compound **2a** or **2b** was converted into the corresponding distannylated monomer **1** or

monomer **2**, which was purified by recrystallization with methanol. For the other co-monomer **3**

or **4**, Stille coupling reaction between compound **4** and tributyl(thiophen-2-yl)stannane yielded

compound **5a** or **5b**. Bromination of compound **5** with N-bromosuccinimide (NBS) in THF gave

the **M3** or **M4**. **M3** is a bright yellow solid, while **M2** is an orange liquid. All the compounds **1-**

5a (5b) and **M1-4** were satisfactorily characterized by[1]H NMR, ^{13}C NMR and elemental

analysis. PBDT-DFQX-PP, PBDT-DFQX-TP, PBDT-DFQX-PT and PBDT-DFQX-TT were

prepared by Stille coupling polymerization reaction between the corresponding monomers

(Scheme 3) catalyzed by Pd$_2$(dba)$_3$/P(*o*-tol)$_3$. The synthesized polymers were purified by

continuous extractions with methanol, hexanes and chloroform, and the chloroform fractions

were recovered. The thiophene π-bridge in the main chain of the polymers was employed to

overcome the steric hindrance between the adjacent donor and acceptor units, and four branched

alkyl chain groups (see Scheme 2) were introduced to ensure the good solubility of the resulting

polymers. As expected, all polymers exhibit good solubility in common organic solvents, such as chloroform, toluene, chlorobenzene, and *o*-dichlorobenzene (DCB). Table 1 summarized the polymerization results and thermal properties of the copolymers. The number-average molecular weight (M_n), weight-average molecular weight (M_w) and the polydispersity index (PDI) of the copolymers, measured by GPC in THF at 30 ℃ using polystyrene standards, showed that the M_n values of PBDT-DFQX-PP, PBDT-DFQX-TP, PBDT-DFQX-PT and PBDT-DFQX-TT are 20.8, 40.1, 24.7, and 44.5 kDa, respectively with PDIs of 2.08, 1.59, 1.63 and 1.82 respectively (Table 1). We note that the molecular weights of the polymers with thienyl side chains are higher compared with their phenyl side chain analogues. In particular the polymer of PBDT-DFQX-TT containing four thienyl side chains, exhibits the highest molecular weight, whereas PBDT-DFQX-PP, which has four phenyl groups, shows the lowest molecular weight and broadest polydispersity. This can be explained by the fact that poor solubility of the growing chain can make polymers precipitate earlier in the reaction preventing further chain growth.[11] These results indicate that the number and nature of the conjugated side-chains have significant influences on the molecular weight of the polymers formed. The thermal transition and stability of polymers were measured by TGA and DSC. DSC scans of the four polymers revealed that there were no obvious phase transitions up to 250℃ (Supporting Information, Figure S1). As shown in Figure 1 and Table 1, TGA thermograms showed that PBDT-DFQX-PP, PBDT-DFQX-TP, PBDT-DFQX-PT and PBDT-DFQX-TT are thermally stable with onset decomposition temperatures corresponding to 5% weight loss at 386, 335, 361, and 402℃, respectively. The results suggest that all the polymers are stable enough for application in PSCs and can be potentially annealed at elevated temperatures.
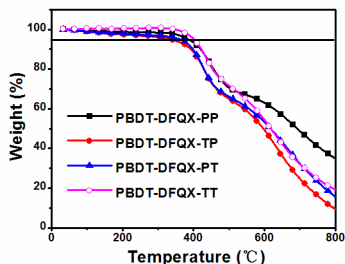
Figure 1. TGA plots of the polymers with a heating rate of 10 ℃/min under an N$_2$ atmosphere.

Table 1. Molecular weights and thermal properties of the polymers

Polymer	yield (%)	Mn (kDa)[a]	M_W(kDa)[a]	PDI	T$_d$ (℃)[b]
PBDT-DFQX-PP	55.4	20.8K	43.2K	2.08	386
PBDT-DFQX-TP	53.2	40.1K	63.9K	1.59	335
PBDT-DFQX-PT	87.6	24.7K	40.4K	1.63	361
PBDT-DFQX-TT	83.4	44.5K	81.3K	1.82	402
[a]Mn, M_W and PDI of the polymers were estimated by GPC using polystyrene as standards in THF . [b] The 5% weight-loss temperatures in nitrogen.					

Optical Properties.

Figure 2 shows the normalized optical absorption spectra of the BDT-DFQX based polymers in dilute chloroform and as thin films deposited on quartz glass. The optical data, including the absorption peak wavelengths (λ_{max}), absorption edge wavelengths (λ_{onset}), and the optical band gap (E_g^{opt}) are summarized in Table 2. Both solution and thin film spectra showed three

characteristic absorption bands. The absorption in the wavelength range of 300-500 nm

originated from the localized π-π* transition, whereas a relatively broad and intense absorption in

the range of 500-700 nm was attributed to the intramolecular charge transfer (ICT) between the

strong electron-accepting fluorinated quinoxaline units (DFQX-P, DFQX-T) and the electron-

donating 2D-BDT units (BDT-P,BDT-T).[12] In the solution spectra, the UV absorption maximum

and the visible ICT peak of the DFQX-T based polymers are red shifted by ca.25nm compared to

the DFQX-P based polymers (Table 1). This could be due to another stronger ICT absorption,

which caused by the more electron-rich thienyl groups pendant onto the central quinoxaline

chromophore.[13] Similar to the solution spectra, the thin film absorption spectra of the polymers

were identical in shape but obvious red-shifts of the absorption maxima (by ca. 30 nm) were

observed, indicating that aggregation of the polymer main chains and π-π intermolecular

interactions occurred in the solid state.[14] However, larger red-shift in λ_{max} from solution to film

for PBDT-DFQX-TT (ca.60 nm) can be observed in comparison with that of the other three

polymers (ca.30 nm). This difference can be ascribed to that, with four conjugated thienyl groups,

PBDT-DFQX-TT is more favorable for the π-π co-facial overlapping perpendicular to polymer

chains.[15] In addition, all the polymers, except PBDT-DFQX-PP, displayed vibronic features at

low- energy absorption band in thin film, implying the presence of ordered π-π stacks, and these

ordered structures favor the charge mobility. The E_g^{opt} of PBDT-DFQX-PP, PBDT-DFQX-TP,

PBD-TDFQX-PT and PBDT-DFQX-TT are 1.83, 1.78, 1.75 and 1.72 eV, respectively,

calculated from the λ_{onset} of solid state films (Table 2). It is worth noting that PBDT-DFQX-TT

displayed the narrowest bandgap, whereas PBD-DFQX-PP displayed the largest bandgap. This

phenomenon could be attributed to the less steric effect, more aggregated conformation and more

electron-rich capability of thienyl side groups in PBDT-DFQX-TT, when contrasted with phenyl

groups in PBDT-DFQX-PP.[16] These results demonstrate convincingly that PBDT-DTQX-TT has

a better ability of light-harvesting, therefore it could achieve a higher J_{sc} than the others when it

is employed to fabricate solar cells as donor materials. Clearly, to construct the BDT-DFQX

based polymers with a more effective chain-chain stacking and a narrower bandgap, it is better to

choose thienyl group as the conjugated side chains both for donor and acceptor units.
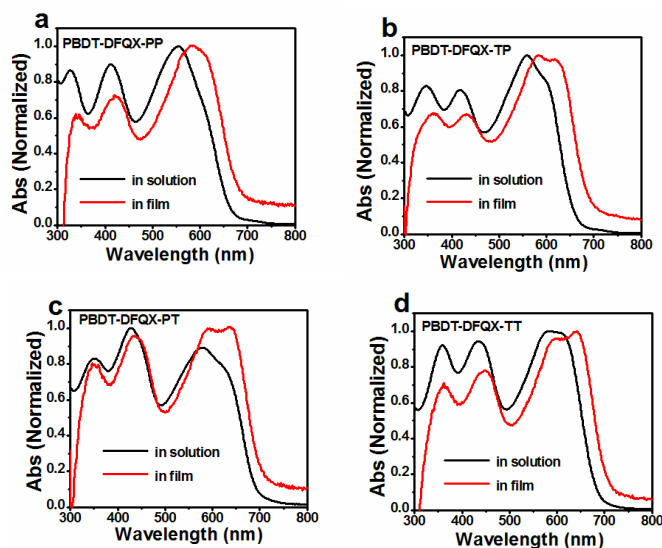

Figure 2. UV/Vis absorption spectra of polymers in CHCl$_3$ solutions and in thin films.

Table 2. Optical and electrochemical properties of the polymers

Polymer	λ^{max}(nm)		λ_{onset}(nm) film	E_g^{opt}(eV)	HOMO(eV)	LUMO (eV)	E_g^{ec}
	solution	film					
PBDT-DFQX-PP	327,413, 554	346,419, 584	678	1.83	-5.35	-3.53	1.82
PBDT-DFQX-TP	347,418, 559	359,431, 583	695	1.78	-5.25	-3.52	1.73
PBDT-DFQX-PT	350,428, 578	347,431, 595	707	1.75	-5.29	-3.58	1.71
PBDT-DFQX-TT	359,435, 586	361,456, 642	717	1.72	-5.20	-3.50	1.70

Electrochemical Properties.

The electronic structures of the four copolymers, viz. highest occupied molecular orbital (HOMO)/lowest unoccupied molecular orbital (LUMO) energy levels, were estimated by cyclic voltammetry.[17] The measured cyclic voltammograms are illustrated in Figure S2 in the Supporting Information and the results are summarized in Table 2. The onset potentials for oxidation (E_{ox}) were observed to be 0.64, 0.58, 0.54 and 0.49 V vs. Ag/Ag$^+$ for PBDT-DFQX-PP, PBDT-DFQX-PT, PBDT-DFQX-TP and PBDT-DFQX-TT, respectively. The onset potentials for reduction (E_{red}) of them were found to be -1.18, -1.13, -1.18 and -1.21 V vs. Ag/Ag$^+$, respectively. The HOMO and LUMO energy levels of the copolymers were calculated from the onset oxidation potential and the onset reduction potential according to the following equations (2) and (3):[18]

$$E_{HOMO} = -e(E_{ox} + 4.71)(eV)$$
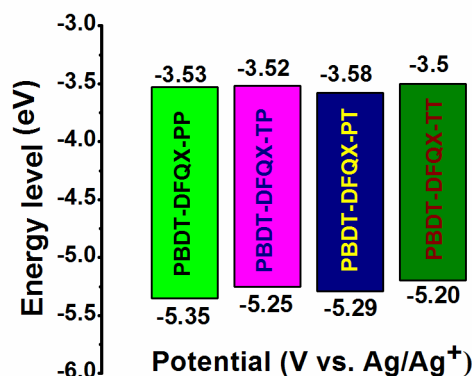
$$E_{LUMO} = -e(E_{red} + 4.71)(eV)$$

Figure 3. Energy level diagrams for the BDT-DFQX-based polymers.

As shown in Figure 3, the LUMO energy levels of PBDT-DFQX-PP, PBDT-DFQX-TP, PBDT-DFQX-PT and PBDT-DFQX-TT, are -3.53, -3.52, -3.58, and -3.50 eV, respectively. Obviously, the LUMO energy levels of the conjugated polymers do not vary appreciably with variation of the conjugated side chains. Meanwhile, all the LUMO energy levels are higher than that of the *n*-type material $PC_{71}BM$ (-3.91eV),[19] ensuring energetically favorable electron transfer. The HOMO energy levels of PBDT-DFQX-PP, PBDT-DFQX-TP, PBDT-DFQX-PT and PBDT-DFQX-TT are estimated to be -5.35, -5.25, -5.29 and -5.20 eV, respectively. Thus one can found that the four copolymers all possess rather low-lying HOMO levels, due to the incorporation of electron-withdrawing fluorine atoms. The low-lying HOMO level is expected

for higher open-circuit voltage (V_{oc}) of the PSCs with the polymers as donor materials because the V_{oc} is usually proportional to the difference between the HOMO level of the donor and the LUMO level of the acceptor. On the other hand, it is worth noting that the HOMO energy levels of the polymers rise gradually as the phenyl conjugated side chains, either on donor or on acceptor units, were replaced by thienyl step by step, and the difference in the HOMO energy level between PBDT-DFQX-TT with all thienyl substituents and PBDT-DFQX-PP with all phenyl substituents is 0.15 eV. The elevation of the HOMO energy level of thienyl substituted copolymers contrasted to phenyl substituted analogues is mainly due to the enhanced electron-donating strength of thiophene compared to benzene.[16] The phenomenon indicates that the conjugated side chains significantly affect the HOMO levels of the D-A copolymers. Also, it can be anticipated that PBDT- DFQX-PP-based PSCs would achieve a higher V_{oc}.

Theoretical Calculations.

To evaluate the impact of the different conjugated side chains on molecular architecture and consequently on the optoelectronic properties of the copolymers, density functional theory (DFT) calculations were performed to verify stationary points as stable states for the optimized conformations and single point energies, with a molecular main chain length n= 1, at b3lyp/6-31g(d,p) level of theory in vacuum using the Gaussian program package. The final energies were calculated as the sum of single point and zero point energies. In particular, the HOMO and LUMO level positions and related electron distributions were calculated. Moreover, all the alkyl chains were replaced by methyl groups in the calculation to avoid excessive computation demand. Optimized geometries of the five copolymers in ground state are shown in Figure S3 (Supporting Information). Calculated dihedral angles and corresponding HOMO, LUMO levels and bandgaps (E_g^{cal}) are summarized in Table 3. The general molecule structure sketch used for

the computational data is shown in Figure 4, where θ_1 is dihedral angle between BDT unit and the side chain groups, θ_2 is dihedral angles between Qx unit and the side chain groups.
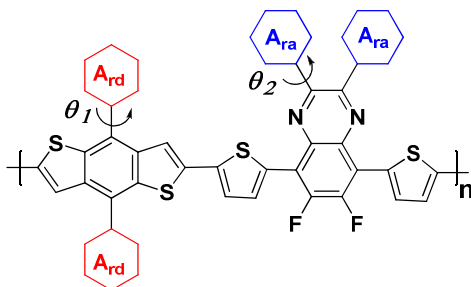

Figure 4. Molecular geometry sketch used for the computational data.

Table 3. Calculated dihedral angles, bond angle and corresponding HOMO, LUMO levels and bandgaps (E_g^{cal}) of the Polymers.

polymer	θ_1(deg)	θ_2(deg)	HOMO(eV)	LUMO (eV)	E_g^{cal} (eV)
PBDT-DFQX	--	--	-4.82	-2.35	2.47
PBDT-DFQX-PP	56.9	45.2	-4.89	-2.32	2.57
PBDT-DFQX-TP	48.7	42.1	-4.87	-2.41	2.46
PBDT-DFQX-PT	62.5	43.5	-4.84	-2.29	2.55
PBDT-DFQX-TT	54.7	40.7	-4.71	-2.27	2.44

Different structures of conjugated side chain groups significantly affect the molecular architecture, as shown in Table 3. The dihedral angles between the conjugated side chain groups and the main chains of polymers are all 40°~60°, indicating twisted conformation of

copolymers. Note that θ_1 and θ_2 in thiophene substituted polymers is smaller than that in benzene substituted polymers, owing to the relatively small bulk of thiophene.[16] The smaller dihedral angles of θ_1 and θ_2 is beneficial to the π-π stacking of polymer main chains. On the other hand, with the side chains varied from PP to TP, to PT then to TT, conformations of the relevant polymers become more planar, which can be beneficial for charge transport. We speculated that this thiophene side groups can be better to form co-planar structure with BDT-DFQX, which is consistent with previous reports.[5a] In this cases, the π-orbital overlap between neighboring polymer main chains are increased, leading to changes in the frontier orbital energy levels and, more specifically, to decrease in band-gaps of thiophene substituted polymers in turn. The wave functions of the frontier molecular orbital are depicted in Figure S4 (Supporting Information). As can be seen in Table 3, although there are some discrepancies between the calculation and experimental results, the calculated HOMO energy levels of the four model compounds also follow the trends of variation: PBDT-DFQX-PP (-4.89 eV) <PBDT-DFQX-TP (-4.87 eV) <PBDT-DFQX-PT (-4.84 eV) <PBDT-DFQX-TT (-4.71 eV). Furthermore, as demonstrated in Figure S4, for all model compounds, the LUMO electron density is mainly located on the acceptors (DFQX-P. DFQX-T), while the HOMO is delocalized along the whole π-conjugated backbone. Similar to CV, the DFT results revealed that benzene substituted polymers have lower HOMO levels and larger electrochemical bandgaps than thiophene substituted polymers.

Photovoltaic Properties.

To investigate the effect of the conjugated side chain pattern on the photovoltaic properties of the copolymers, the devices were fabricated with the ITO/PEDOT: PSS/polymer: $PC_{71}BM$/Ca/Al structure. The polymer and $PC_{71}BM$ was dissolved into *o*-dichlorobenzene to make the D-A mixed solution for spin-coating. The device fabrication process is described in detail in the

Experimental Section. Different weight ratios of polymer: $PC_{71}BM$ and thicknesses of the active layers were carefully optimized. The measurements of photovoltaic performances were carried out under illumination of AM1.5G simulated solar light at 100 mW·cm^{-2}. The corresponding open-circuit voltage (V_{oc}), short circuit current (J_{sc}), fill factor (FF), and power conversion efficiency (PCE) of the devices are summarized in Table 4, while Figure 5 shows the representative current density-voltage (J-V) curves of the best devices. The detailed photovoltaic data of the optimization process for the PSCs are listed in Table S1 in the Supporting Information.
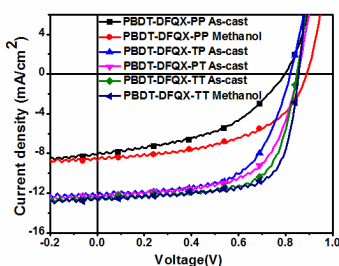

Figure 5. Current density-voltage characteristics of the PSCs based on polymer:$PC_{71}BM$ blends under illumination of AM1.5G, 100 mW·cm^{-2}.
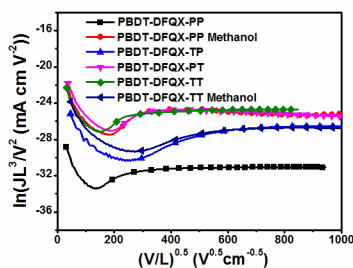

Figure 6. Plots of $\ln(JL^3/V^2)$ versus $(V/L)^{0.5}$ for the measurement of the hole mobility in polymer/$PC_{71}BM$ devices by the SCLC method.

Table 4. Photovoltaic performances of the PSCs based on polymer/$PC_{71}BM$ under the illumination of AM1.5G, 100 mW·cm^{-2}

Polymer	Ratio[a]	V_{oc}(V)	J_{sc}(mA/cm^2)	FF (%)	PCE[c](%)	Mobility $(cm^2V^{-1}s^{-1})$[d]
PBDT-DFQX-PP	1:2	0.80	8.11	45.60	2.96	1.10×10^{-4}
PBDT-DFQX-PP	1:2[b]	0.89	8.66	51.38	3.96	8.85×10^{-4}
PBDT-DFQX-TP	1:1	0.82	12.34	60.12	6.08	1.33×10^{-3}
PBDT-DFQX-PT	1:1	0.85	12.13	63.46	6.54	2.94×10^{-3}
PBDT-DFQX-TT	1:1.2	0.85	12.53	68.51	7.29	4.09×10^{-3}
PBDT-DFQX-TT	1:1.2[b]	0.86	12.77	69.93	7.68	6.28×10^{-3}

[a]Polymer/$PC_{71}BM$ weight ratio. [b]Treatment with methanol.[c] Optimized data.

[d] Measured by using the SCLC method.

As shown in Table 4, under the optimal conditions without any treatment and solvent additive, the highest PCE of the devices were 2.96%, 6.08%, 6.54% and 7.29% for PBDT-DFQX-PP, PBDT-DFQX-TP, PBDT-DFQX-PT and PBDT- DFQX- TT, respectively. As shown in Figure 5 and Table 4, PBDT-DFQX-PP exhibited a lower J_{sc} of 8.11mA·cm^{-2}, most likely due to a relatively broad band gap and blue-shifted absorption, whereas the J_{sc}s of the other three polymers were relatively higher, in the range of 12.13~12.53 mA·cm^{-2}. On the other hand, it can be observed in Table S1, the V_{oc} of devices decreased from 0.89 V to 0.85 V, owing to the upshift of the HOMO levels from PBDT-DFQX-PP to PBDT-DFQX-TT. An increase in the $PC_{71}BM$ content also resulted in a slight decrease in the V_{oc} and these results are in accordance

with previously reported ones.[20]Although the introduction of phenyl side chains successfully enhances the V_{oc} of PBDT-DFQX-PP-based device, this is not sufficient to offset the reduction in J_{sc} and FF, especially for an unsatisfactory FF of 45%, leading to a disappointing PCE of 2.96%. It is interesting to note that thienyl substituted polymers exhibit superior photovoltaic properties achieving PCE of >6.50% to phenyl substituted ones, especially, the polymers with thienyl side chains on acceptor units possess better performance than those polymers with thienyl side chains on donor units, and lowering the ratio of thienyl in the conjugated side chains leads to lower performance: as the proportion of thienyl side chains decreased from 100% to 50% to 0, the maximum PCE dropped from 7.29% to 6.54% to 6.08%, then to 2.96%. Thus, the PBDT-DFQX-TT-based device exhibits the highest PCE of 7.29% at the optimized film thickness of 110 nm, which is 2.5 times higher than that of the PBDT- DFQX-PP-based device. This phenomenon indicates that thienyl side chains are more beneficial to achieve high PCEs of relevant polymers, which, on the one hand, can be attributed to the higher hole mobilities of thienyl substituted polymers (the hole mobilities were shown in table 4 and Figure 6), on the other hand, can be ascribed to the excellent self-aggregation and proper phase separation of thiophene side chains substituted polymers when blended with $PC_{71}BM$.[5a] It is well-known that processing additives, such as1,8-diiodooctane (DIO), 1-chloronaphthalene (CN) can dramatically enhance device performance. Thus we also checked the effect of DIO or CN additive on the four copolymers. Disappointingly, when an amount of DIO or CN(3%, v/v) was added as the processing additive, the results showed the additive of DIO or CN has no positive effect on the device performance of the four polymers. PCE of the relevant devices exhibited a slight reduction due to the decrease of V_{oc} or FF (Table S1).

Table 5. Characteristics of PBDT-DFQX-TT-based PSCs under different processing conditions

Ratio[a]	1:1	1:1.2	1:1.5	1:2	1:3	1:1[b]	1:1.2[b]	1:1.5[b]
Mobility(cm^{2}V^{-1}s^{-1})[c]	3.15×10^{-3}	4.09×10^{-3}	3.73×10^{-3}	3.89×10^{-3}	2.53×10^{-3}	1.66×10^{-3}	6.28×10^{-3}	7.08×10^{-3}
FF (%)	69.15	68.51	67.90	69.92	69.07	64.49	69.93	70.79
PCE (%)[d]	7.16	7.29	6.99	6.92	5.62	7.36	7.68	7.41

[a] Polymer/PC$_{71}$BM weight ratio. [b] Treatment with methanol.

[c] Measured by using the SCLC method. [d] Optimized data.

Inspired by recent work on post-solvent treatment,[21] we tried to employ methanol to further optimize the performance of PSCs with a modified procedure:(i) spin-coated the active layer and dried under vacuum; (ii) 60μl methanol was added atop the active layer and 30 seconds was allowed; (iii) solvent was removed by spin coating at high speed (3000 rpm); (iv)the Ca/Al was evaporated (as shown in experimental section). From Table 4 and Table S1 in the Supporting Information, one can observe that different polymers showed different performance for the methanol treatment. Cheerfully, for PBDT-DFQX-PP and PBDT-DFQX-TT, photovoltaic performance of the two polymers had been enhanced to some extent, achieving PCE$_{max}$ of 3.96% and 7.68% respectively. To date 7.68% is one of a few Qx-based PSCs which exhibited PCE exceeding 7.5%. It is worthwhile to note that the FF of PBDT-DFQX-PP was enhanced from 45% to 51% after methanol treatment, as well as the hole mobility was promoted to 8.85×10^{-4} from 1.10×10^{-4} cm^{2}V^{-1}s^{-1}. These might be originated from the relatively low surface resistance of PBDT-DFQX-PP blend films,[22] which caused by methanol. Figure S5 (Supporting Information) shows the hole mobilitiy, FF and PCE of the PBDT-DFQX-TT-based PSCs under

different processing conditions and the results are summarized in Table 5. As demonstrated by Figure S5 and Table 5, it appears that PBDT-DFQX-TT is a star polymer, its PSC achieved high fill factor of > 62.0% and promising PCE of > 5.6% at a relative broad weight ratio of polymer/$PC_{71}BM$. Meanwhile, the hole mobility of all relevant devices based on PBDT-DFQX-TT keep the value of 10^{-3} $cm^2V^{-1}s^{-1}$, and the high hole mobility partially account for stable and high J_{sc} and FF values. So with four thienyl side chains, the PBDT-DFQX-TT demonstrated the best photovoltaic performance with an excellent PCE of 7.68%. However for those BDT-DFQX-based polymers reported in literature, in which the optimized conjugated side chains were attached either on donor or acceptor units, the relative PSCs just exhibited the highest PCE of 6.1%.[23] Based on the above obtained experimental results, we can conclude that optimizing the conjugated side chains both on donor and on acceptor units synchronously would be a more effective strategy to improve the photovoltaic properties of BDT-DFQX-containing copolymers.
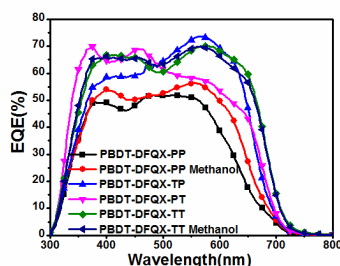

Figure 7. EQE spectra of the PSCs based on polymer/$PC_{71}BM$ blends.

The external quantum efficiency (EQE) curves of the devices fabricated under the optimal conditions are shown in Figure 7. It can be noted that the EQE responses of all the polymers in the visible region can be attributed to both the intrinsic absorption of the polymers and the response of $PC_{71}BM$. Among them, the device based on PBDT-DFQX-PP/$PC_{71}BM$ (1:2, w/w) exhibits a response range from 350 nm to 650 nm and a relatively low EQE value, with two

maximum peak values of 49% at~384nm and of 51% at ~520nm. After methanol treatment, EQE of PBDT-DFQX-PP is slightly improved both in long wavelength region and in short wavelength one, which should be ascribed to the change of microstructure of blend film. However, compared with the PBDT-DFQX-PP-based device, the other devices show a significant improvement of EQE in the wavelength range 400-600 nm, with the peak values exceeding 70%. For the convenience of analysis, the absorption spectra of the blend films prepared by the optimal conditions were shown in Figure S6 (Supporting Information). One can see that the shapes of the EQE spectra of the devices are similar to the absorption spectra of their active layer used. The blend films showed remarkably broad absorption in the range of 300-450 nm mainly due to the $PC_{71}BM$ absorption in this region. The absorption ability of PBDT-DFQX-TP and PBDT-DFQX-TT based devices were stronger than that of others from 500 to 700 nm. The high EQE and enhanced optical absorption of the active layer means more efficient photoelectron conversion in this range, hence benefits for the improvement of J_{sc}. The difference in EQE and absorption spectra curves under the optimal conditions result in the different J_{sc} values of the devices. These results were consistent with the data in J-V measurements, and the difference between the J_{sc} and the integral of the EQE by the solar irradiation spectrum, AM 1.5G, was~4%, which provided the solid evidence for the reliability of the photovoltaic results.
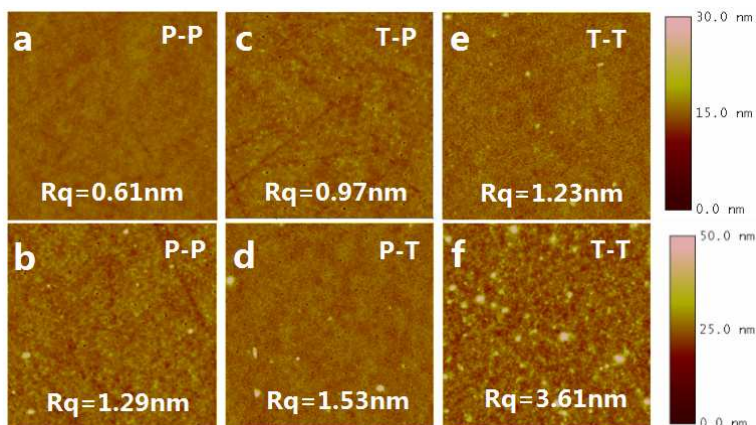
Microstructure

Figure 8. Topographic AFM images ($5\times5\mu m^2$) of the blend films of PBDT-DFQX-PP/PC$_{71}$BM 1:2 w/w (a, without methanol treatment; b, with methanol treatment);PBDT-DFQX-TP/PC$_{71}$BM 1:1 w/w (c); PBDT-DFQX-PT/PC$_{71}$BM 1:1 w/w (d); PBDT-DFQX-TT/PC$_{71}$BM 1:1.2 w/w (e, without methanol treatment; f, with methanol treatment).

To investigate the effect of microstructure of polymer/PC$_{71}$BM films on device performance, AFM, TEM and GIXS measurements were performed. The surface morphology recorded by tapping mode AFM is shown in Figure 8 (topography images). Under the conventional conditions, all polymers display uniform and smooth films, with a small root-mean-squared (RMS) of 0.61~1.53 nm. In contrast, the treatment of methanol for the PBDT-DFQX-PP increased the RMS of blend film from 0.61 nm to 1.29 nm (see Figure 8 a, b). Similar to PBDT-DFQX-PP, the surface of the active layer became clearly rougher with increasing RMS of 1.23 to 3.61nm for PBDT- DFQX-TT after the methanol treatment (see Figure 8 e, f). The larger RMS probably resulted from the enhanced aggregation of the donor polymers and acceptor fullerene in the active layer. Although polar solvent treatment did not provide an adequate driving force for reconstructing the morphologies of the polymer films, some of the polar solvent could penetrate the active layer.[24] After wetting for 30 seconds, PC$_{71}$BM particles could be redistributed to

reduce the contact areas with methanol and led to sufficient aggregations with donor polymers. Consequently, the formation of phase separation of the blend films occurred. The nanoscale morphologies of polymer/$PC_{71}BM$ films were further studied using TEM. As seen in Figure 9 a, large-scale phase separation could be observed and the clear phase boundary of PBDT-DFQX-PP/$PC_{71}BM$ is chapped and discontinuous, which is harmful to exciton diffusion, exciton separation and charge transport. Thus, PBDT-DFQX-PP-based device achieved both a relative low J_{sc} and FF. Unlike the film of PBDT-DFQX-PP/$PC_{71}BM$, a nanoscale interconnected network structure between fibril-like PBDT-DFQX-PP and $PC_{71}BM$ is well developed in 1 : 1.2 ratio film (see Figure 8 d). The well developed interconnected network structure affords not only high J_{sc} but also excellent FF. However, it could be observed that the PBDT-DFQX-TP or PBDT-DFQX-PT blend film exhibits moderately homogeneous and there were no evidence of detrimental scale phase segregation, indicating that both of them possessed good miscibility with $PC_{71}BM$ (see Figure 8 b, c). It also resulted in the satisfactory PCEs of corresponding devices.
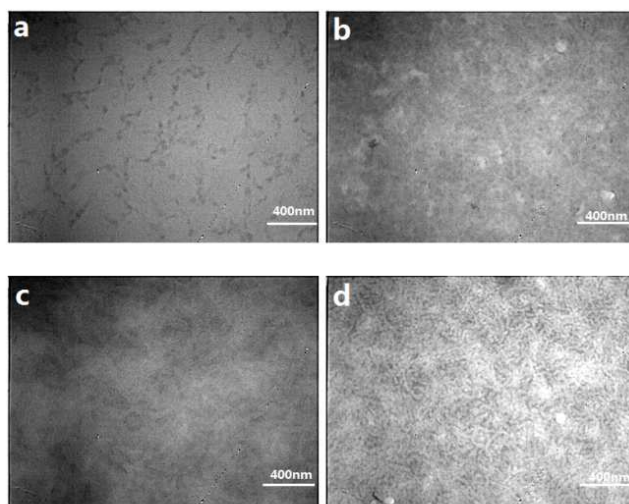

Figure 9. TEM images of the blend films of PBDT-DFQX-PP/$PC_{71}BM$ (a); PBDT-DFQX-TP/$PC_{71}BM$ (b); PBDT-DFQX-PT/$PC_{71}BM$ and PBDT-DFQX-TT/$PC_{71}BM$.
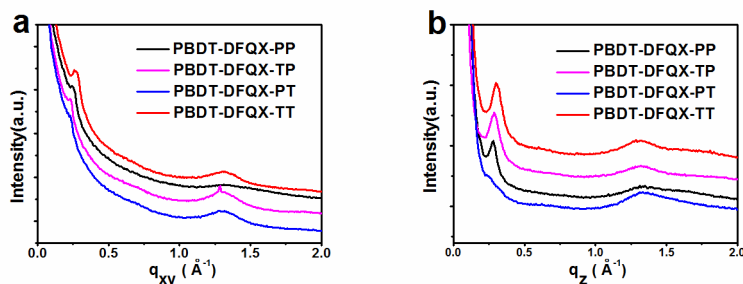
Figure 10. GIXS of polymer/PC$_{71}$BM blended thin film (a) in-plane, (b) Out-of-plane.

To gain deeper insight of the crystallinity and molecular organization of the polymer thin films,

X-ray diffraction analysis (XRD) of the pristine polymer films was performed. As shown in

Figure S7 (Supporting Information), for all polymers, a relatively weak diffraction peak can be

observed at about 2θ= 22.8-23.4°, which corresponds to the π-π stacking distances ($d_{\pi\text{-}\pi}$= 3.79-

3.91 Å) between coplanar conjugated polymers. Compared with PBDT-DFQX-PP ($d_{\pi\text{-}\pi}$= 3.91

Å), PBDT-DFQX-TT ($d_{\pi\text{-}\pi}$= 3.79 Å) displayed an enhanced intensity diffraction as well as a

shortening of the π-π stacking distance. Interestingly, PBDT-DFQX-TT thin film exhibited a

clear diffraction peak at 2θ= 3.7°, corresponding to the lamellar distance of 23.80 Å. While no

relative diffraction peaks were detected in other three polymer films. The results reveal that the

film of PBDT-DFQX-TT has a relatively order structure and stronger intermolecular interactions,

[25] which can be partly supported by the observation from the UV spectra, where PBDT-DFQX-

TT shows the strongest vibrational peak at long wave direction. All these differences could be

due to the less steric hindrance between thienyl side groups and the neighboring groups of

another molecule.[26] In order to further understand the microstructures of polymers, the

preferential orientation of the blend films was investigated by GIXS. Figure 10a and 10b shows

in-plane (IP) and the out-of-plane (OOP) GIXS profiles of the blend films, including PBDT-

DFQX-PP/PC$_{71}$BM blend (1:2, w/w, treated with methanol), PBDT-DFQX-TP/ PC$_{71}$BM blend

(1:1, w/w), PBDT-DFQX-PT/PC$_{71}$BM blend (1:1, w/w) and PBDT-DFQX-TT /PC$_{71}$BM blend

(1:1.2, w/w, treated with methanol) cast from *o*-DCB (10 mg/ml), respectively. As shown in

Figure 10, for all the blend films, both the OOP (100) and IP (100) reflections could be observed.

However, the stronger intensity of the (100) reflection in the OOP profile than in the IP profile

indicated that the lamellar packing BDT-DFQX-based polymers preferentially stacked out of the

film plane (edge-on rich orientation), though with some randomness. The results may be

attributed to the introduction of branched alkyl side-chains in polymers resulting in the

misorientation of the polymer lamellae. [27] When compared with XRD patterns of the pristine

polymer films (Figure S7), it is noteworthy that a clear lamellar diffraction peak could be

observed in the GIXS profiles (Figure 10). Additionally, stacking peaks in GIXS profiles became

sharper and more intense than those in XRD patterns upon blending with $PC_{71}BM$, suggesting

that structures of the blend films became more ordered. The result may arise from the strong

polymer-fullerene interactions that delay the fullerene self-assembly in the final drying process.[28]

Consequently, fullerene could induce polymer self-assembly towards the kinetics equilibration of

the blends' phase separation.[29] The IP profile of the blend films showed a pronounced (100)

diffraction peak at 0.235, 0.237, 0.244, and 0.265Å^{-1}, for PBDT-DFQX-PP, PBDT-DFQX-TP,

PBDT-DFQX-PT and PBDT-DFQX-TT respectively, corresponding to the conjugated side chain

packing distance of 26.74, 26.51, 25.75, and 23.71 Å. Thus, we can conclude that the polymers

with thienyl side chains exhibit a shorter interchain distance than those with phenyl side chains.

Due to the strong polymer-fullerene interactions, the reflection of polymers corresponding to the

π- π stacking peak overlapped with the $PC_{71}BM$ peak.[30] In addition, we can observe that

intensities of the π- π and lamellar stacking peaks increased gradually from PBDT-DFQX-PP to

PBDT-DFQX-TT (Figure 10). This phenomenon indicated that a relatively higher degree of

crystallinity formed for PBDT-DFQX-TT, which coincides with the images estimated from TEM

(see Figure 8 d). Moreover, the smaller lamellar spacing of PBDT-DFQX-TT relative to the phenyl side-chain derivatives benefits charge transport across domains as well as π-electron hopping among the polymer chains. [31] Obviously, the tighter packing and higher degree of crystallinity of PBDT-DFQX-TT correspond well with the enhanced value of hole mobility and FF (Table 4 and Table 5). These results suggest that the presence of large amounts of thienyl side chains contribute to highly ordered structure and effective charge transport, leading to PBDT-DFQX-TT with a promising PCE of 7.68%. Whereas phenyl side chains suppress the aggregation of BDT-DFQX polymers in the solid state, which may hinder the charge carrier transport of the blend film of polymer and $PC_{71}BM$, resulting in PBDT-DFQX-PP with a moderate PCE of 3.98%.

CONCLUSION

In this work, four BDT-DFQX-based derivatives were synthesized and characterized to investigate the effect of conjugated side chain modulation on photovoltaic properties. In these four polymers, different side chain combinations including *p*-alkoxyphenyl and *p*-alkoxyphenyl (PP), 2-alkylthienyl and *p*-alkoxyphenyl (TP), *p*-alkoxyphenyl and 2-alkylthienyl (PT), 2-alkylthienyl and 2-alkylthienyl (TT) were used to tune the photoelectronic properties. DFT calculations reveal that the thiophene side groups show weaker steric hindrance and smaller dihedral angle to the backbones than that of benzene side groups. The difference of the steric bulk, electron-donating ability and aromaticity between thiophene and benzene appeared to greatly affect the morphology, charge transport and photovoltaic performance of devices. The photovoltaic results indicate that PBDT-DFQX-TT and PBDT-DFQX-PP show totally different photovoltaic characteristics in device, and PCEs of 7.68% and 3.96% were obtained, respectively. Whereas devices incorporating PBDT-DFQX-TP or PBDT-DFQX-PT with

$PC_{71}BM$ exhibited PCEs of 6.08% or 6.54% .This can be ascribed to the enhanced interchain π-π stacking effect and well-developed fibril structure of PBDT-DFQX-TT-based device. This work could provide some insight into side chain engineering to construct efficiently photovoltaic polymers.

EXPERIMENTAL SECTION

Materials

Scheme 2 shows the synthetic routes to the copolymers. Monomers 2,6-Bis(trimethyltin)-4,8-bis(4-ethylhexyloxy-1-phenyl)-benzo[1,2-b:4,5-b']-dithiophene (**M1**),[10a] 2,6-Bis(trimethyltin)-4,8-bis(5-(2-ethylhexyl)thiophen-2-yl)-benzo[1,2-b:4,5-b']-dithiophene (**M2**),[10b] 5,8-Bis(5-(2-ethylhexyl)thiophen-2-yl)-6,7-difluoro-2,3-bis(4-(ethylhexyloxy)phenyl)quinoxaline (**M3**)[10c] and 5,8-Bis(5-(2-ethylhexyl)thiophen-2-yl)-6,7-difluoro-2,3-bis(5-ethylhexythiophen-2-yl) quinoxaline (**M4**)[9b] were synthesized according to literature procedures. Tetrahydrofuran (THF) was dried over Na/benzophenoneketyl and freshly distilled prior to use. Other reagents and solvents were of commercial grade and used as received without further purification. All reactions were performed under a nitrogen atmosphere.

Synthetic Procedures

Synthesis of poly{4,8-bis(4-ethylhexyloxy-1-phenyl)-benzo[1,2-b:4,5-b']- dithiophene-alt-5,8-bis(5-thiophen-2-yl)-6,7-difluoro-2,3-bis(4- (ethylhexyloxy) phenyl)quinoxaline} (PBDT-DFQX-PP)

A mixture of 0.1 mmol of **M1** (92.45 mg) and an equal quantity of **M3** (89.70 mg) were mixed in 6 mL of degassed chlorobenzene. After being purged with nitrogen for 15 min, $Pd_2(dba)_3$

(0.005 mol, 5 mg) and P(*o*-tol)$_3$ (0.005 mol ,12.5 mg) were added and the mixture was then purged with nitrogen for another 15 min. The reaction mixture was vigorously stirred at 130℃ for 48 h. When the reaction mixture was cooled to room temperature, the polymer was precipitated by slow dropwise addition into methanol (200 mL), collected by filtration and washed with methanol. Then the solid was subjected to Soxhlet extraction with methanol, hexane, and chloroform. The polymer was recovered as solid from the chloroform fraction by precipitation from methanol, filtered off, and dried to afford PBDT-DFQX-PP copolymer as a bronze black solid (74 mg, 55.4%). M_n=20.8 kDa; M_W=43.2 kDa; PDI=2.08; ^{1}H NMR (600 MHz, CDCl$_3$): δ (ppm) 7.94-7.28 (br, 14 H), 7.18-6.83 (br, 10 H), 3.99-3.89 (br, 8 H), 1.82-0.64 (br, 60 H); Elemental analysis calcd (%) for (C$_{82}$H$_{92}$N$_2$F$_2$O$_4$S$_4$)$_n$: C 73.73, H 6.94, N 2.10, S 9.60; found: C73.29, H7.32, N 2.27, S 9.17.

Synthesis of poly{4,8-bis(5-(2-ethylhexyl)thiophen-2-yl)benzo[1,2-b:4,5-b']dithiophene-alt-5,8-bis(5-thiophen-2-yl)-6,7-difluoro-2,3-bis(4-(ethylhexyloxy) phenyl)quinoxaline} (PBDT-DFQX-TP)

   PBDT-DFQX-TP was synthesized and purified following the same procedure for PBDT-DFQX-PP, but monomer **M2** (90.45 mg, 0.1 mmol) was used instead of **M1**. PBDT-DFQX-TP was obtained as a black solid (70 mg, 53.2%). M_n=40.1 kDa; M_W=63.9 kDa; PDI=1.59; ^{1}H NMR (600 MHz, CDCl$_3$): δ (ppm) 7.80-7.43 (br, 10 H), 7.09-6.87 (br, 8 H), 3.92-3.64 (br, 8 H), 1.93-0.69 (br, 62 H); Elemental analysis calcd (%) for (C$_{78}$H$_{88}$N$_2$F$_2$O$_4$S$_6$)$_n$: C 71.19, H 6.74, N 2.13, S 14.62; found: C 72.03, H 6.32, N 2.07, 14.93.

Synthesis of poly{4,8-bis(4-ethylhexyloxy-1-phenyl)-benzo[1,2-b:4,5-b']- dithiophene-alt-5,8-bis(5-thiophen-2-yl)-6,7-difluoro-2,3-bis(5-ethylhexythiophen-2-yl)quinoxaline} (PBDT-DFQX-PT)

PBDT-DFQX-PT was synthesized and purified following the same procedure for PBDT-DFQX-PP, but monomer **M4** (87.70 mg, 0.1 mmol) was used instead of **M3**. PBDT-DFQX-PT was obtained as a black solid (118 mg, 90%). M_n=24.7 kDa; M_W=40.4 kDa; PDI=1.63; ^{1}H NMR (600 MHz, CDCl$_3$): δ (ppm) 8.02-7.37 (br, 10 H), 7.13-6.67 (br, 8 H), 3.95-3.84 (br, 8 H), 1.83-0.72 (br,62 H); Elemental analysis calcd (%) for $(C_{78}H_{88}N_2F_2O_4S_6)_n$: C 71.99, H 6.74, N 2.89, S 14.62; found: C 71.65, H7.31, N 2.77, S 14.31.

Synthesis of poly{4,8-bis(5-(2-ethylhexyl)thiophen-2-yl)-benzo[1,2-b:4,5-b']- dithiophene-alt-5,8-bis(5-thiophen-2-yl)-6,7-difluoro-2,3-bis(5-ethylhexythiophen-2- yl)quinoxaline} (PBDT-DFQX-TT)

PBDT-DFQX-TT was synthesized and purified following the same procedure for PBDT-DFQX-TP, but monomer **M4** (87.70 mg, 0.1 mmol) was used instead of **M3**. PBDT-DFQX-TT was obtained as a dark black solid (114 mg, 87.9%). M_n=44.5 kDa; M_W=81.3 kDa; PDI=1.82; ^{1}H NMR (600 MHz, CDCl$_3$): δ (ppm) 7.67-7.40 (br, 8 H), 7.08-6.62 (br, 6 H), 3.32-2.91 (br, 8 H), 1.84-0.63 (br, 62 H); Elemental analysis calcd (%) for $(C_{74}H_{84}N_2F_2O_4S_8)_n$: C 68.58, H 6.53, N 2.93, S 19.79; found: C 69.05, H 5.92, N 2.78, S 20.13.

Characterization

^{1}H and ^{13}C-NMR spectra were recorded on a Bruker AV600 spectrometer using CDCl$_3$ as the solvent. Elemental analyses were performed on a Flash EA 1112 analyzer. Molecular weights of

the polymers were measured by gel permeation chromatography (GPC) method on Waters 515-2410 with polystyrenes as standard and tetrahydrofuran (THF) as an eluent. Differential scanning calorimetry (DSC) measurements were performed using a METTLER differential scanning calorimeter (DSC822e) range from 25-250 ℃ under nitrogen at a heating rate of 10 ℃·min^{-1}. Thermogravimetric analysis (TGA) was conducted on a Netzsch TG209C analyzer at a heating rate of 10 ℃·min^{-1}. UV/Vis absorption spectra were measured on solutions of polymer in chloroform and on polymer films cast onto quartz glass by using a Shimadzu model UV-3150 spectrometer. Electrochemical cyclic voltammetry was conducted on a Zahner IM6e electrochemical workstation with a Pt disk coated with the polymer film, Pt plate, and Ag/Ag^{+} electrode as the working electrode, counter electrode, and reference electrode, respectively, in a 0.1 mol·L^{-1} solution of Bu_4NPF_6 in acetonitrile. All solutions were purged with nitrogen for 20 minutes before each experiment. AFM characterization of the surface morphology of the active blend layers was done on a Nano scope V AFM (Digital Instruments) system using tapping mode in air. AFM images were recorded directly on the tested devices, in the device area out of the Ca/Al electrode. Transmission electron microscope (TEM) images were obtained using a JEOL 2200FS transmission electron microscope operated at accelerating voltage of 200 kV. Thin films were first floated on deionized water and then transferred onto copper grid. The samples were dried at room temperature for 2 h before TEM experiments. Thin films were drop-cast on a glass substrate for X-ray diffraction (XRD) and grazing incidence X-ray scattering (GIXS). X-ray diffraction (XRD) measurements of thin neat polymer films were performed in reflection mode with Cu Kα radiation (40 kV, 40 mA; λ= 0.15418 nm) using a Bruker AXSD8 focus diffractometer. For grazing incidence X-ray scattering (GIXS), the drop-cast blend films were illuminated at a constant incidence angle of 0.2°. Scattering intensities are expressed as a

function of the scattering vector, $q=4\pi/\lambda\sin\theta$, where θ is the half scattering angle and $\lambda=1.57\text{Å}$ is the wavelength of the incident radiation. The d-spacing of a peak is expressed by $2\pi/q$. Molecular simulation was carried out for copolymers, with a chain length of n=1 at the b3lyp/6-31g(d,p) level with the Gaussian program package.

Fabrication and Characterization of Photovoltaic Devices.

PSC with the device structure of ITO/PEDOT:PSS/polymer: $PC_{71}BM$ blend/Ca/Al were fabricated. ITO/glass substrates were cleaned sequentially in ultrasonic baths of acetone, deionized water, 2-propanol, and then dried at 150°C for 15 min in air. ITO/glass substrates were treated with oxygen plasma before use. A thin layer of poly(3,4-ethylenedioxythiophene): polystyrene sulfonate (PEDOT:PSS) was spin-cast on precleaned ITO-coated glass from a PEDOT:PSS aqueous solution (Baytron P VP AI 4083 from H.C. Starck) at 3000 rpm and dried subsequently at 150°C for 30 min in a vacuum oven, then the device was transferred to a glovebox, where the active layer of the blend of the polymer and (6,6)-phenyl C_{71} butyric acid methyl ester ($PC_{71}BM$) was spin-coated onto the PEDOT:PSS layer. Finally, a Ca/Al metal top electrode was deposited in vacuum onto the active layer by vacuum evaporation under 2×10^{-4} Pa. The active area of the device was ca. 4 mm^2. The thickness of the photosensitive layer was ca. 60-120nm, measured on an Ambios Tech XP-2 profilometer. The current density-voltage (*J-V*) characteristics were measured on a computer-controlled Keithley 236 Source-Measure Unit. A xenon lamp (150 W) coupled with AM 1.5 solar spectrum filter was used as the light source, and the optical power at the sample was 100 $mW\cdot cm^{-2}$. External quantum efficiency (EQE) spectrum was measured by a Stanford Research Systems model SR830 DSP lock-in amplifier coupled with WDG3 monochromator and a 150 W xenon lamp. The devices for the hole

mobility measurement were fabricated using the architectures:

ITO/PEDOT:PSS/polymer:$PC_{71}BM$/Au. The hole mobilities were calculated by fitting the

current density-voltage ($J-V$) curves using the Mott-Gurney relationship (space-charge limited

current, SCLC). The SCLC can be approximated by the equation (1):

$$J = \frac{9}{8}\varepsilon_r\varepsilon_0\mu_0 \exp\left(0.891\,\gamma\sqrt{\frac{V}{L}}\right)\frac{V^2}{L^3} \quad (1)$$

Here J is the current density, ε_r is the dielectric constant of the polymer, ε_0 is the free-space

permittivity (8.85×10^{-12} F/m), μ_0 is the charge mobility at zero field, γ is a constant, L is the

thickness of the blended film layer, $V = V_{appl} - V_{bi}$, V_{appl} is the applied potential, and V_{bi} is the built-

in potential which results from the difference in the work function of the anode and the cathode

(in hole device architecture, $V_{bi} = 0.2$ V).

Acknowledgements

REFERENCES

(1) (a) J. M. Szarko, J. Guo, Y. Liang, B. Lee, B. S. Rolczynski, J. Strzalka, T. Xu, S. Loser, T. J. Marks, L. Yu and L. X. Chen, *Adv. Mater*, **2010**, *22*, 5468. (b) G. Yu, J. Gao, J. C. Hummelen, F. Wudl and A. J. Heeger, *Science*, **1995**, *270*, 1789. (c) J. Chen and Y. Cao, *Acc. Chem. Res*, **2009**, *42*, 1709. (d) G. Dennler, M. C. Scharber and C. J. Brabec, *Adv. Mater*, **2009**, *21*, 1323.

(2) (a) S. Q. Zhang, L. Ye, W. C. Zhao, D. L. Liu, H. F. Yao and J. H. Hou, *Macromolecules*, **2014**, *47*, 4653. (b) L. Ye, S. Q. Zhang, W. C. Zhao, H. F. Yao and J. H. Hou, *Chem. Mater*, **2014**, *26*, 3603.

(3) (a) S. H. Park, A. Roy, S. Beaupre, S. Cho, N. Coates, J. S. Moon,D. Moses, M. Leclerc, K. Lee and A. J. Heeger, *Nat. Photonics*, **2009**, *3*, 297. (b) N. Wang, Z. Chen, W. Wei, and Z. H. Jiang, *J. Am. Chem. Soc*, **2013**, *135*, 17060. (c) H. L. Zhong, Z. Li, F. Deledalle, E. C. Fregoso, M. Shahid, Z. P. Fei, C. B. Nielsen, N. Y. Gross, S. Rossbauer, T. D. Anthopoulos, J. R. Durrant, and M. Heeney, *J. Am. Chem. Soc*, **2013**, *135*, 2040.

(4) (a) Facchetti. A, *Chem. Mater*, **2010**, *23*, 733. (b) J. H. Kim, C. E. Song, B. S. Kim, I. N. Kang, and D. H. Hwang, *Chem. Mater*, **2014**, *26*, 1234. (c) L. X. Wang, D. D. Cai, Q. D. Zheng, C. Q. Tang, S. C. Chen and Z. G. Yin, *ACS Macro Lett*, **2013**, *2*, 605. (d) Y. F. Li, *Acc. Chem. Res*, **2012**, *45*, 723.

(5) (a) H. M. Qin, L. S. Li, T. X. Liang, X. B. Peng, J. B. Peng, Y. Cao, *J. Polym. Sci, Part A: Polym. Chem*, **2013**, *51*, 1565. (b) J. M. Jiang, H. K. Lin, Y. Che. Lin, H. C. Chen, S. C. Lan, C. K. Chang and K. H. Wei, *Macromolecules*, **2014**, *47*, 70.

(6) (a) Yang. L, Zhou. H, You. W, *J. Phys. Chem. C*, **2010**, *114*, 16793. (b) Szarko. J. M,Guo. J, Liang. Y, Lee. B, Rolczynski. B. S, Strzalka. J, Xu. T, Loser. S, Marks. T. J, Yu. L, Chen. L. X, *Adv. Mater*, **2010**, *22*, 5468.

(7) (a) R. F. He, L. Yu, P. Cai, F. Peng, J. Xu, L. Ying, J. W. Chen, W. Yang and Y. Cao, *Macromolecules*, **2014**, *47*, 2921. (b) M. Tessarolo, D. Gedefaw, M. Bolognesi, F. Liscio, P. Henriksson, W. Zhuang, S. Milita, M. Muccini, E. Wang, M. Seri, M. R. Andersson, *J. Mater. Chem*. *A*, **2014**, *2*, 11162. (c) D. F. Dang, W. C. Chen, S. Himmelberger, Q. Tao, A. Lundin, R.

Q. Yang, W. G. Zhu, A. Salleo, C. Müller, E. G. Wang, *Adv. Energy Mater*. **2014**, DOI: 10.1002/aenm.201400680.

(8) (a) L. L. Han, X. C. Bao, T. H, Z. K. Du, W. C. Chen, D. Q. Zhu, Q. Liu, M. L. Sun, R. Q. Yang, *Macromol. Rapid Commun*, **2013**, *35*, 1153. (b) J. H. Kim, M. J. Lee, H. C. Yang and D. H. Hwang, *J. Mater. Chem. A*, **2014**, *2*, 6348. (c) M. J. Zhang, X. Guo, W. Ma, S. Q. Zhang, L. J.Huo, H. Ade and J. H. Hou, *Adv. Mater*, **2014**, *26*, 2089. (d) J. Warnan, C. Cabanetos, R. Bude, A. E. Labban, L. Li and Pierre M. Beaujuge, *Chem. Mater*, **2014**, *26*, 2829. (e) M. J. Zhang, Y. Gu, X. Guo, F. Liu, S. Q. Zhang, L. J. Huo, T. P. Russell, and J. h. Hou, *Adv. Mater*, **2013**, 25, 4944.

(9) (a) R. M. Duan, L. Ye, X. Guo, Y. Huang, P. Wang, S. Q. Zhang, J. P. Zhang, L. J. Huo, J. H. Hou, *Macromolecules*, **2012**, *45*, 3032. (b) M. Wang, S. W. Shi, D. Ma, K. L. Shi, C. Gao, L. W. Wang, G. Yu, Y. F. Li, X. Y. Li and H. Q. Wang, *Chem. Asian J*, **2014**, DOI: 10.1002/asia.201402564.

(10) (a) L. T. Dou, J. Gao, E. Richard, J. B. You, C. C. Chen, K. C. Cha, Y. J. He, G. Li, Y. Yang, *J. Am. Chem. Soc*, **2012**, *134*, 10071. (b) L. J. Huo, S. Q. Zhang, X. Guo, F. Xu, Y. F. Li, J. H. Hou, *Angew. Chem. Int. Ed*, **2011**, *50*, 9697. (c) S. Li, Z. C. He, J. Yu, S. A. Chen, A. S. Zhong, H. B. Wu, C. Zhong, J. G. Qin, Z. Li, *J. Polym. Sci, Part A: Polym. Chem*. **2012**, *50*, 2819.

(11) H. L. Zhong, Z. Li, Ester. B. D, S. Rossbauer, S. E. Watkins, N. Stingelin, T. D. Anthopoulos, M. Heeney, *J. Mater. Chem. A*, **2013**, *1*, 14973.

(12) E. Zhou, J. Cong, K. Tajima and K. Hashimoto, *Chem. Mater*. **2010**, *22*, 4890.

(13) Y. Y. Lai, Y. J. Cheng, C. H. Chen, S. W. Cheng, F. Y. Cao and C. S. Hsu, *Polym. Chem*, **2013**, *4*, 3333.

(14) Huo. L, Ye. L, Wu. Y, Li. Z, Guo. X, Zhang. M, Zhang. S, Hou, J. *Macromolecules*. **2012**, *45*, 6923.

(15) X. L. Feng, V. Marcon, W. Pisula, M. R. Hansen , J. Kirkpatrick, F. Grozema, D. Andrienko, K. Kremer, K. Müllen, *Nature Materials,* **2009**, *8*, 421.

(16) Z. G. Zhang and J. Z. Wang, *J. Mater. Chem*, **2012**, *22*, 4178.

(17) Li. Y. F, Cao. Y, Gao. J, Wang. D. L, Yu. G, Heeger. A. J, *Synth. Met*. **1999**, *99*, 243.

(18) Zhao. G, He. Y, Li. Y, *Adv. Mater*. **2010**, *22*, 4355.

(19) He. Y. J, Li. Y. F, *Phys. Chem. Chem. Phys*, **2011**, *13*, 1970.

(20) Veldman. D, Meskers. S. C. J, Sweelssen. J, Koetse. M. M, Veenstra. S. C, Kroon. J. M, Bavel. S. S, Loos. J, Janssen. R. A. J, *J. Am. Chem. Soc*, **2008**, *130*, 7721.

(21) (a) Wang. Y, Liu. Y, Chen. S, Peng. R, Ge. Z, *Chem. Mater*, 2013, 25, 3196. (b) Zhou. H, Zhang. Y, Seifter. J, Collins. S. D, Luo. C, Bazan. G. C, Nguyen. T. Q, Heeger. A. J, *Adv. Mater*, **2013**, *25*, 1646. (c) P. Shen, H. J. Bin, L. Xiao and Y. F. Li, *Macromolecules*, **2013**, *46*, 9575.

(22) Y. Wang, F. Yang, Y. Liu, R. X. Peng, S. J. Chen and Z. Y. Ge, *Macromolecules*, **2013**, *46*, 1368.

(23) (a) M. Bolognesi, D. Gedefaw, D. F. Dang, P. Henriksson, W. L. Zhuang, M. Tessarolo, E. G. Wang, M. Muccini, M. Seri and M. R. Andersson, *RSC Adv*, **2013**, *3*, 24543. (b) M. L. Keshtov, D. V. Marochkin, V. S. Kochurov, A. R. Khokhlov, E. N. Koukarasand G. D. Sharma,

Polym. Chem, **2013**, *4*, 4033. (c) J. H. Kim, C. E. Song, H. U. Kim, A. C. Grimsdale, S. J. Moon, W. S. Shin, S. K. Choi and D. H. Hwang, *Chem. Mater*, **2013**, 25, 2722. (d) H. C. Chen, Y. H. Chen, C. H. Liu, Y. H. Hsu, Y. C. Chien, W. T. Chuang, C. Y. Cheng, C. L. Liu, S. W. Chou, S. H. Tung and P. T. Chou, *Polym. Chem*, **2013**, *4*, 3411.

(24) Nam. S, Jang. J, Cha. H, Hwang. J, An. T. K, Park. S, Park. C. E, *J. Mater. Chem*, **2012**, *22*, 5543.

(25) I. Osaka, S. J. Shinamura, T. Abe, K. Takimiya. *J. Mater. Chem. C*, **2013**, *1*, 1297.

(26) (a) H. X. Zhou, L. Q. Yang, W. You, *Macromolecules*. **2012**, *45*, 607. (b) J. G. Mei and Z. N. Bao, *Chem. Mater*, **2014**, *26*, 604.

(27) I. Osaka, R. Zhang, J. Liu, D-M. Smilgies, T. Kowalewski and R. D. McCullough, *Chem. Mater*, **2010**, 22, 4191.

(28) (a) B. Schmidt-Hansberg, M. Sanyal, M. F. G. Klein, M. Pfaff, N. Schnabel, S. Jaiser, A. Vorobiev, E. Muller, A. Colsmann, P. Scharfer, D. Gerthsen, U. Lemmer, E. Barrena and W. Schabel, *ACS Nano*, **2011**, 5, 8579. (b) J. Rivnay, S. C. B. Mannsfeld, C. E. Miller, A. Salleo and M. F. Toney, *Chem. Rev*, **2012**, 112, 5488.

(29) (a) H-C. Chen, I-C. Wu, J-H. Hung, F-J. Chen, I-W. P. Chen, Y-K. Peng, C-S. Lin, C-h. Chen, Y-J. Sheng, H-K. Tsao and P-T. Chou, *Small*, **2011**, 7, 1098. (b) A. C. Mayer, M. F. Toney, S. R. Scully, J. Rivnay, C. J. Brabec, M. Scharber, M. Koppe, M. Heeney, I. McCulloch and M. D. McGehee, *Adv. Funct. Mater*, **2009**, 19, 1173.

(30) F. Liu, W. Zhao, J. R. Tumbleston, C. Wang, Y. Gu, D. Wang, A. L. Briseno, H. Ade, and T. P. Russell, *Adv. Energy Mater*. **2014**, DOI: 10.1002/aenm.201301377. (b) Y. Huang, E. J. Kramer, A. J. Heeger, and G. C. Bazan, *Chem. Rev*, **2014**, 114, 7006.

(31) (a) Y. J. Cheng, S. H. Yang, C. S. Hsu, *Chem. Rev*. **2009**, *109*, 5868. (b) S. Gu, H. Neugebauer, N. S. Sariciftci, *Chem. Rev*. **2007**, *107*, 1324.

For "Table of Content" only

The Role of Conjugated Side Chains in High Performance Photovoltaic Polymers

Meng Wang [1,2], Di Ma [1], Keli Shi[1,3], Shaowei Shi [1], Song Chen[4], Changjiang Huang [1], Zi Qiao[1], Zhi-Guo Zhang[3], Yongfang Li[3]*, Xiaoyu Li[1]*, and Haiqiao Wang[1.2]*